

EFFECT OF INTERNAL FLOWS ON SUNYAEV-ZELDOVICH MEASUREMENTS OF CLUSTER PECULIAR VELOCITIES

DAISUKE NAGAI^{1,2}, ANDREY V. KRAVTSOV^{1,2}, ARTHUR KOSOWSKY^{1,3}
Draft version December 12, 2018

ABSTRACT

Galaxy clusters are potentially powerful probes of the large-scale velocity field in the Universe because their peculiar velocity can be estimated directly via the kinematic Sunyaev-Zeldovich effect (kSZ). Using high-resolution cosmological simulations of an evolving cluster of galaxies, we evaluate how well the average velocity obtained via a kSZ measurement reflects the actual cluster peculiar velocity. We find that the internal velocities in the intracluster gas are comparable to the overall cluster peculiar velocity, 20 to 30% of the sound speed even when a cluster is relatively relaxed. Nevertheless, the velocity averaged over the kSZ map inside a circular aperture matched to the cluster virial region provides an unbiased estimate of a cluster's radial peculiar velocity with a dispersion of 50 to 100 km/s, depending on the line of sight and dynamical state of the cluster. This dispersion puts a lower limit on the accuracy with which cluster peculiar velocity can be measured. Although the dispersion of the average is relatively small, the velocity distribution is broad; regions of low signal must be treated with care to avoid bias. We discuss the extent to which systematic errors might be modelled, and the resulting limitations on using galaxy clusters as cosmological velocity tracers.

Subject headings: cosmology: theory – intergalactic medium – methods: numerical – galaxies: clusters: general – instabilities – turbulence – X-rays: galaxies: clusters

1. INTRODUCTION

Accurate maps of the cosmic velocity field would provide powerful constraints on the formation of structure in the Universe. A velocity field can be compared directly with measured galaxy density field, testing whether the fundamental picture of gravitational collapse is correct (Branchini et al. 2001; da Costa et al. 1998; Doré et al. 2002), or with velocity fields predicted by cosmological models, providing useful constraints on cosmological parameters and an independent measurement of the bias parameter on a range of scales. Indeed, intensive theoretical effort in the last decade produced very accurate predictions of various properties of the velocity fields from the linear to the highly nonlinear regime (e.g., Jing & Boerner 1998; Freudling et al. 1999; Juszkiewicz et al. 1999; Colín et al. 2000). However, despite clear theoretical importance, velocity surveys have been overshadowed by recent redshift surveys because peculiar velocities are far more difficult to measure than redshifts. Existing velocity surveys are thus more prone to systematic errors than redshift surveys. The main difficulty in measuring peculiar velocity is, of course, obtaining the distance to an object, which is necessary if the peculiar velocity is obtained by subtracting the Hubble flow velocity from a measured redshift velocity. Since distance errors tend to increase with distance, the reliability of redshift-based peculiar velocity surveys inevitably degrades with distance, making cosmological tests on large scales difficult.

Several groups have proposed using clusters of galaxies as tracers of the cosmic velocity field (Haehnelt & Tegmark 1996; Lange et al. 1998; Kashlinsky & Atrio-Barandela 2000; Aghanim et al. 2001; Peel & Knox 2002).

The peculiar velocity of a cluster can be measured in a single step, independent of the cluster distance, via the kinematic Sunyaev-Zeldovich effect (SZE : Zeldovich & Syunaev 1969; Sunyaev & Zel'dovich 1980); for recent reviews see Birkinshaw (1999) and Carlstrom et al. (2002). The electrons of the hot ionized gas in clusters Compton-scatter passing microwave background photons, resulting in a frequency-dependent redistribution of the photon energies (the thermal SZ effect). A smaller but measurable blackbody distortion arises from the Doppler shift due to bulk motion of the electrons with respect to the rest frame of the CMB photons (the kinematic SZ effect, hereafter kSZ). In principle, these effects can be distinguished by their spectral signatures. With sufficiently high angular resolution observations the kSZ signal can be distinguished from intrinsic microwave background temperature fluctuations because galaxy clusters subtend angular scales small compared to characteristic primordial fluctuations. First measurements of the kSZ signal in clusters have been reported (Holzapfel et al. 1997), and several studies of the systematic errors related to disentangling the kSZ signal from other microwave fluctuations have been performed (Haehnelt & Tegmark 1996; Aghanim et al. 2001; Diego et al. 2002).

If clusters were simple spherical objects with negligible internal structure and motions (as has been assumed in several previous papers investigating the effect), then measurements of the kinematic SZ effect would provide a relatively straightforward method for measuring the cluster peculiar velocity. However, we know from high-resolution X-ray observations (i.e., Markevitch et al. 2000; Vikhlinin et al. 2001; Sun & Murray 2002; Mazzotta et al. 2002) and

¹ Center for Cosmological Physics, University of Chicago, Chicago IL 60637

² Department of Astronomy and Astrophysics, University of Chicago, 5640 S. Ellis Ave, Chicago IL 60637

³ Department of Physics and Astronomy, Rutgers University, 136 Frelinghuysen Road, Piscataway, NJ 08854-8019

numerical simulations (i.e., Norman & Bryan 1999; Ricker & Sarazin 2001) that galaxy clusters are actually complex objects with significant internal flows driven by frequent mergers. The observed kinematic SZ signal, which measures the density-weighted peculiar velocity of gas, will thus be some average over the bulk velocity and the internal velocities, which raises the question of how accurately an observed SZ signal will reflect the actual peculiar velocity of the cluster. Potential systematic errors can arise because the gas itself does not necessarily reflect the bulk velocity of the matter.

In this paper we use high-resolution simulations of a galaxy cluster formed in a Λ CDM cosmological model to investigate the systematic errors that can arise from the complex internal structure and motion in estimates of the cluster velocity via the kSZ effect. In §2, we describe the cluster simulation used in our analysis. In §3, we illustrate the structure and magnitude of internal flows within the cluster. §4 explains how to estimate the peculiar velocity from kSZ maps, discusses definitions of peculiar velocity and analyzes the systematic errors in the kSZ estimate. We summarize our results and discuss related issues in the final section.

2. NUMERICAL SIMULATIONS

We analyze a high-resolution cluster simulation performed using the Adaptive Refinement Tree (ART) N -body+gasdynamics code (Kravtsov 1999; Kravtsov et al. 2002). ART is an Eulerian code designed to achieve high spatial resolution by adaptively refining regions of interest, such as high-density regions or regions of steep gradients in gas properties, and has good shock-capturing characteristics. The code can capture discontinuities in gas properties within $\sim 1 - 2$ grid cells without using artificial viscosity, which makes it well-suited for studying sharp features such as shock fronts and studying velocity fields. At the same time, adaptive refinement in space and (non-adaptive) refinement in mass (Klypin et al. 2001) allows us to reach the large dynamic range required for high-resolution self-consistent simulations of cluster evolution in a cosmological setting.

The effects of magnetic fields, gas cooling, stellar feedback, and thermal conduction are not included in these simulations. As we show below, the systematic errors in the measurements of the radial peculiar velocity of clusters from kSZ observations arise mainly from the proximity of merging sub-clumps and the internal turbulent motion of cluster gas induced by mergers. These dynamical processes are expected to be largely unaffected by the neglected physical processes. More importantly, properly assessing the effect of gas flows requires simulations of cluster formation in a realistic cosmological setting, taking into account non-spherical accretion of matter along filaments along with major and minor mergers which induce the internal gas motions. The simulation analyzed here follows formation of a galaxy cluster from CDM initial conditions and has both very high mass and spatial dynamic range to model accurately the small-scale dynamics of dark matter and gas.

Specifically, we analyze a simulation of a cluster of intermediate mass in a Λ CDM model with $\Omega_m = 1 - \Omega_\Lambda = 0.3$, $\Omega_b = 0.043$, $h = 0.7$ and $\sigma_8 = 0.9$, where the Hubble con-

stant is defined as $100h \text{ km s}^{-1} \text{ Mpc}^{-1}$, and σ_8 is the rms density fluctuation on $8h^{-1} \text{ Mpc}$ scales. The simulation used a base 128^3 uniform grid and 7 levels of mesh refinement in a computational box of $80h^{-1} \text{ Mpc}$ with a peak formal resolution of $5h^{-1} \text{ kpc}$ and mass resolution (particle mass) of $2.7 \times 10^8 h^{-1} M_\odot$. At $z = 0$, the cluster has virial mass of $M_{340} = 2.4 \times 10^{14} h^{-1} M_\odot$ and virial radius of $R_{340} = 1.26h^{-1} \text{ Mpc}$, where the subscripts indicate the cosmology-dependent virial overdensity with respect to the mean density of the Universe. This Λ CDM cluster simulation was recently used in the analysis of “cold fronts” in clusters (Nagai & Kravtsov 2002), and further numerical details of the cluster simulation can be found there.

3. INTERNAL FLOWS

The main question we want to answer is the extent to which the internal flows intrinsic to clusters will degrade measurements of cluster peculiar velocities inferred from the kSZ effect. We start by illustrating the structure and magnitude of internal flows using the high-resolution simulation of a galaxy cluster described above.

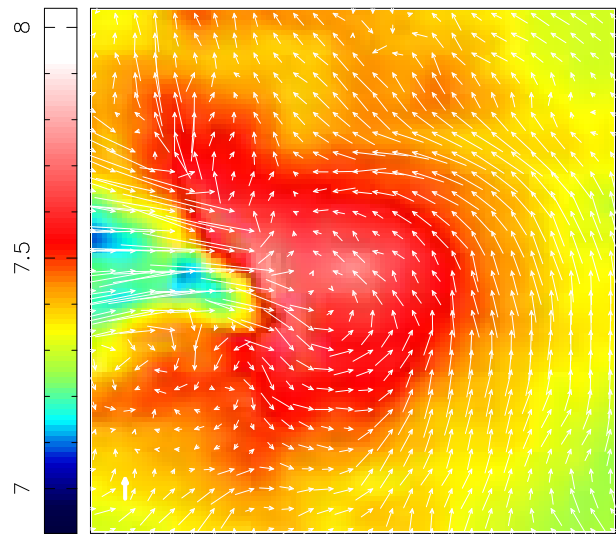


FIG. 1.— A gas velocity map overlaid on the emission-weighted temperature map of the cluster at $z = 0$. The gas velocity is the average projected velocity in a $78h^{-1} \text{ Mpc}$ slice centered on the central density peak. The comoving size of the region is $0.82h^{-1} \text{ Mpc}$. The length of the thick vertical vector in the bottom-left corner corresponds to 300 km s^{-1} ; the temperature maps are color-coded on a \log_{10} scale in units of degrees Kelvin.

Figure 1 shows velocity maps of gas overlaid on the emission-weighted temperature map of a relatively relaxed cluster at $z = 0$. The velocity map shows the average gas velocity in a $78h^{-1} \text{ kpc}$ slice centered on the central density peak; the comoving size of the displayed region is $0.82h^{-1} \text{ Mpc}$. The velocity map shows internal bulk motions of gas at a level of $\sim 200 \text{ km s}^{-1}$ within this relaxed cluster. The typical flow velocities are $\sim 10 - 30\%$ of the sound speed in the cluster core. Gas motions of a similar magnitude in the cores of relaxed clusters are implied by the Chandra observations (Markevitch et al. 2002). Note the merging sub-clump with velocity $\gtrsim 1000 \text{ km s}^{-1}$ on the left side of the main cluster. Regions of fast-moving gas are generally present even in “relaxed” clusters due to ongoing minor mergers. These prominent internal motions are potential sources of bias in the peculiar velocity estimate.

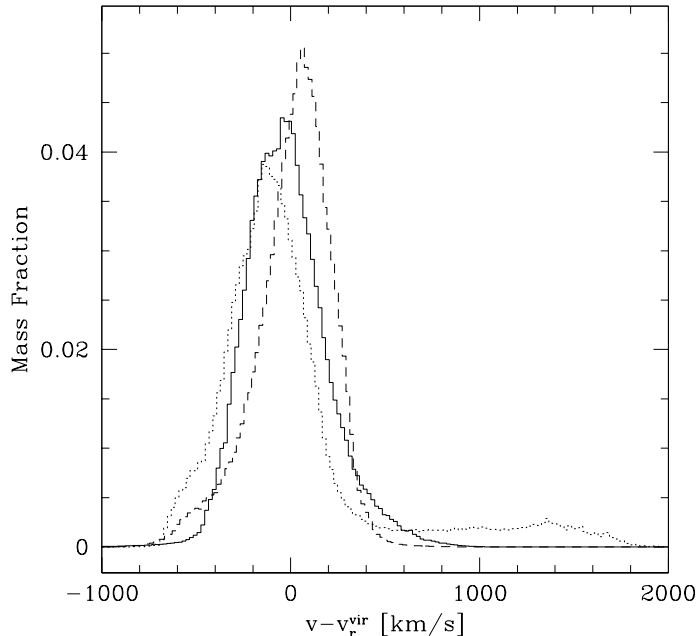


FIG. 2.— The distribution of the gas velocity component along three orthogonal projections within the virial radius of the cluster at $z = 0$. (Solid, dotted, and dashed lines correspond to the left, middle, and right panel projections in Fig. 3 below.)

Figure 2 shows the distribution of the gas velocity component along three orthogonal projections within the virial radius of the cluster at $z = 0$. The velocity distributions are Gaussian with velocity dispersion of $\sim 200 \text{ km s}^{-1}$, except for one case where a merging sub-clump has a line-of-sight velocity $\gtrsim 1000 \text{ km s}^{-1}$ (see also Fig. 1). The symmetric nature of the velocity distribution indicates that the kSZ velocity estimate will generally reflect the true peculiar velocity, but that merging high-velocity substructures along the line of sight can bias the measurements, even given an exact recovery of the kSZ signal. Our simulation suggests that such substructure occurs in a non-negligible fraction of clusters.

4. PECULIAR VELOCITIES FROM THE KINEMATIC SZ EFFECT

Can we measure the radial peculiar velocity of clusters using the kSZ effect accurately enough to learn about cosmology? In the previous section, we have demonstrated that internal gas motion and fast-moving merging sub-clumps are generally present even in the relaxed cluster with velocities comparable to the overall cluster peculiar velocity. So, sizable systematic errors are expected in the peculiar velocity estimate via kSZ effect, even if a recovery of the kSZ signal is perfect. This raises a question of how accurately the kSZ signal will reflect the actual peculiar velocity of cluster. To address this issue, we assume the exact recovery of the kSZ signal and construct noiseless kSZ distortion maps from the high-resolution cluster simulation at different epochs and along three orthogonal directions. We then estimate radial peculiar velocities from these maps and compare the value to the radial peculiar velocity of a cluster defined by the smoothed dark matter distribution.

Note that the question addressed here is separate from

the question of how well the kSZ signal can actually be extracted from a realistic map, both technically and conceptually. Other uncertainties, particularly confusion with the lensing signal and point source contamination, will give systematic errors in the estimate of the kSZ signal itself, which will propagate into peculiar velocity estimates. These error sources will be considered elsewhere. The error we estimate below is the *irreducible* peculiar velocity error due to internal motions of the intracluster gas.

4.1. Simulated kSZ Maps

The kSZ effect arises due to Compton scattering of CMB photons by ionized gas in motion with respect to the rest frame of the CMB. The resulting induced temperature fluctuation is

$$-\frac{\Delta T}{T}(\vec{x}) = b(\vec{x}) \equiv \sigma_T \int dl n_e v_r, \quad (1)$$

where σ_T is the Thompson cross section, n_e is the electron number density, v_r is the velocity component along the line of sight (in units of the speed of light), the integration is along the line of sight, and \vec{x} represents directions on the (flat) sky. We generate kSZ maps of the simulated cluster from uniform density and velocity grids centered on the minimum of cluster potential by numerically integrating Eq. 1. The density and velocity grids, in turn, were constructed using interpolation from the original mesh refinement structure. We then model measurements at a given resolution by convolving the maps with a Gaussian beam profile $A_\sigma(r)$ of appropriate width. Throughout this paper, we will assume a FWHM beamwidth of 1 arcminute. While individual clusters will be observed with higher resolution than this, it is unlikely that large SZ cluster surveys useful for cosmology will obtain significantly higher resolution in the near future. Higher resolution would not significantly alter our conclusions since the dominant systematic effects are unrelated to whether fine-scale structure is resolved in the maps.

Figure 3 shows kSZ maps of the simulated cluster at two different cosmic times (corresponding to redshifts $z = 0.43$ and $z = 0$) in three orthogonal projections (the left panel corresponds to the projection in Fig. 1). The top panels show the raw kSZ maps of a simulated cluster, with the earlier time in the top row. The size of the region shown in the figure is $2h^{-1}$ comoving Mpc and the region is centered on the minimum of cluster potential. The comoving pixel size of the grid is $2h^{-1} \text{ Mpc}/256 \approx 8h^{-1} \text{ kpc}$, close to the spatial resolution of the simulation. The bottom panels show the kSZ maps shown in the top panels convolved with a 1 arcminute FWHM Gaussian beam, assuming a cluster angular diameter distance corresponding to a redshift of $z = 0.1$. One arcminute corresponds to the physical scale $77.5h^{-1} \text{ kpc}$ at $z = 0.1$ in the adopted ΛCDM cosmology. The smoothed maps are heavily oversampled, with a pixel size around a tenth of the beam width. All maps are color-coded on a \log_{10} scale.

The high-resolution kSZ maps show a complex spatial structure of the kSZ distortion signal associated with internal motion of cluster gas and merging subclumps seen in Fig. 1. At $z = 0.43$, the cluster is in a dynamically active stage; two nearly equal-mass sub-clusters have just undergone a slightly off-axis major merger and created strong merger shocks. In the top-left panel of Fig. 3, fast-moving

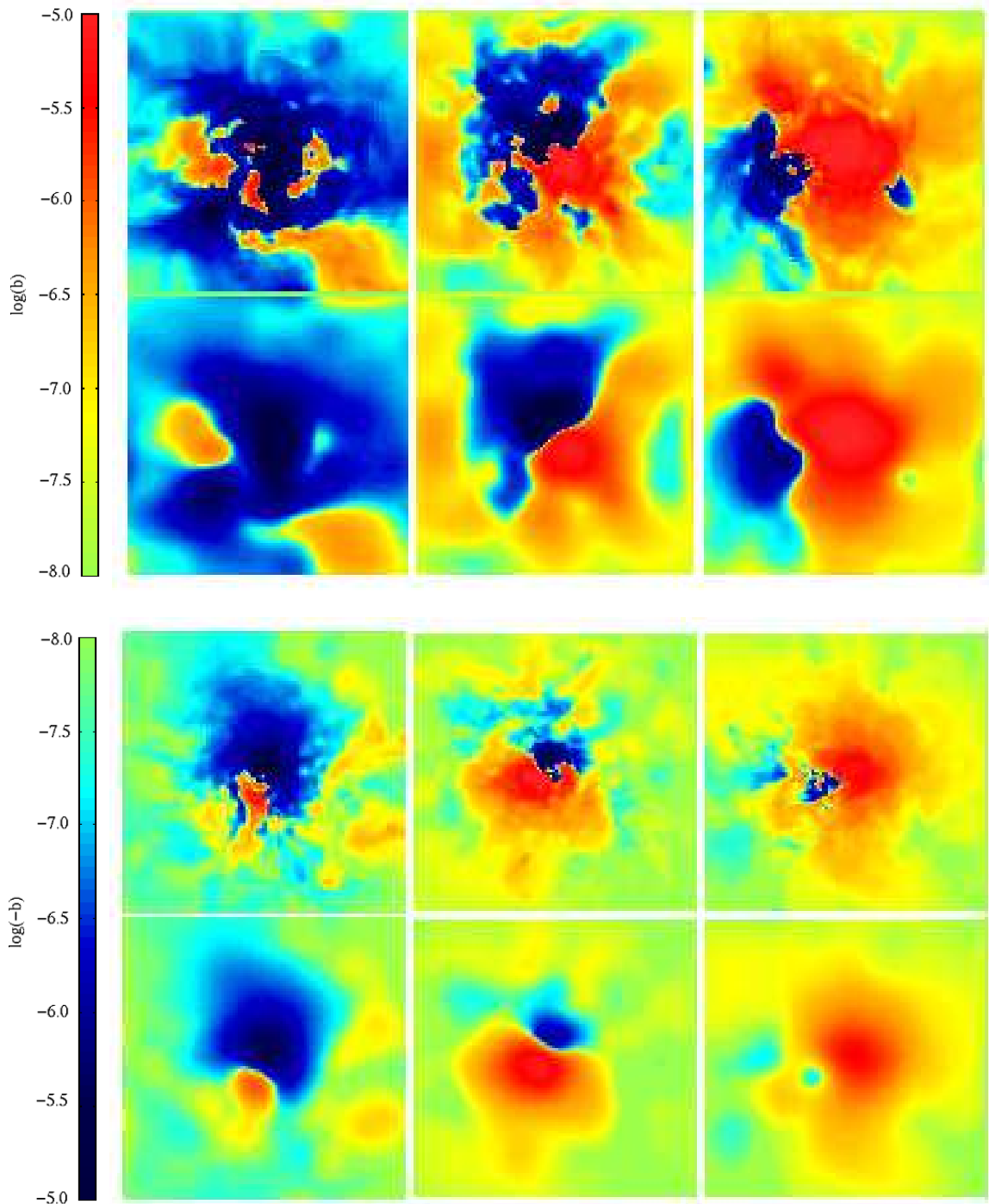


FIG. 3.— *First and third rows:* noiseless kinematic SZ Effect (kSZ) maps of the simulated Λ CDM cluster at redshifts $z = 0.43$ (1st row) and $z = 0$ (2nd row) through three orthogonal projections. *Second and fourth rows:* the kSZ maps shown in the top panels convolved with a $1'$ (FWHM) Gaussian beam, assuming the cluster is at a distance corresponding to redshift $z = 0.1$. The maps are color-coded on a \log_{10} scale which is shown on the left hand side of the plots. The comoving size of the region shown is $2h^{-1}$ Mpc centered on the minimum of cluster potential, and the comoving pixel size is around $8h^{-1}$ kpc. Note that 1 arcminute corresponds to the physical scale $85 h^{-1}$ kpc at $z = 0.1$.

gas ($\gtrsim 1000$ km/s) associated with the merger shock fronts appears as a large positive kSZ signal at the locations where the shock fronts are present, while the cluster as a whole is moving away from the observer, resulting in an overall negative kSZ signal when the raw kSZ signal is convolved with the Gaussian beam. In the top-middle panel

of Fig. 3, the merger axis is aligned parallel to the line-of-sight direction, and the merger shock fronts propagating in both directions of the merger axis result in a dipole pattern in the kSZ signal. At $z = 0$, the cluster is in a relatively relaxed state, but continues to accrete matter and undergo minor mergers. In the bottom-middle panel,

the merging subclump from Fig. 1 is moving parallel to the line of sight, appearing as the strongly negative kSZ signal. This behavior is generic for galaxy clusters in our simulations: even epochs where the cluster is “relaxed” minor merger(s) are typically present (see also Fig. 2). The ever-present internal motions within the cluster produce prominent substructure in the kSZ maps.

4.2. Estimating Radial Peculiar Velocity from kSZ Maps.

How do we estimate the cluster peculiar velocity from a kSZ map? The most straightforward approach is to define some aperture centered on the cluster center (i.e., the peak of the thermal SZ signal or X-ray emission) and calculate the average velocity within the aperture. As we discuss below, this *aperture average velocity* is, in fact, a largely unbiased estimator of a cluster’s radial peculiar velocity, and the error in each measurement will depend on the size and shape of the aperture used to select the cluster region for the analysis. For accurate velocity measurements, the aperture must be chosen large enough to encompass the bulk of the cluster region, and the optimal aperture is matched to the virial radius of the cluster.

To construct a radial velocity estimator from the beam-smearred kSZ maps, we assume that all of the gas in the cluster is moving with a single radial bulk velocity. To compute the aperture average velocity from the maps, we first define a circular aperture centered on the minimum of cluster potential and calculate the beam-smearred kSZ flux $\langle b^B \rangle$ using all pixels within the aperture. In practice, the minimum of the gravitational potential is very close to the maximum of the cluster X-ray emission or SZ signal. Using the same set of pixels, we also calculate the average beam-smearred electron column density $\langle \tau^B \rangle$. The estimated radial velocity is then simply

$$v_r^{\text{est}} = \frac{c}{\sigma_T} \frac{\langle b^B \rangle}{\langle \tau^B \rangle} \quad (2)$$

Below, we consider three different apertures relative to the cluster virial radius: $r_{\text{vir}}/4$, $r_{\text{vir}}/2$, and r_{vir} and compute $\langle \tau^B \rangle$ in two different ways. In the context of a simulation, it is simple to compute this quantity directly from the line of sight average of optical depth. Observationally, one needs to estimate the thermal SZ effect and measure cluster gas temperature to determine the beam-smearred column density, $\langle \tau^B \rangle = (m_e c^2 / \sigma_T k_B) \times [\langle y^B \rangle / \langle T_e \rangle_{n_e}^B]$. However, the density-weighted electron temperature $\langle T_e \rangle_{n_e}^B$ is not an observable; instead, the emission-weighted temperature of cluster gas $\langle T_X \rangle$ from the X-ray spectroscopy is often used. If the intracluster medium is isothermal throughout, then $\langle T_e \rangle_{n_e}^B = \langle T_X \rangle$. Departures from isothermality will give some systematic error in this approximation. To mimic the situation that will arise in the analysis of the actual observations, we also compute $\langle \tau^B \rangle$ based on observables assuming that the intracluster medium is isothermal throughout and evaluating $\langle T_X \rangle$ within each aperture for the 0.5-2.0keV band, using the Raymond & Smith (1977) plasma emission model and assuming a uniform metallicity of 0.3 solar.

4.3. Definitions of Peculiar Velocity

To gauge the accuracy of estimated radial velocity from kSZ maps in the previous section, we need to define a reference “true” radial peculiar velocity. In the literature,

the peculiar velocity is typically defined to be the density-weighted average dark matter velocity within a sphere of some characteristic cluster radius. The most natural outer boundary of a cluster is given by the virial radius, but a fixed radius is also often used in the literature (e.g., Abell radius of 1.5 Mpc Bahcall et al. 1994; Croft & Efstathiou 1994; Colberg et al. 2000). We define v_r^{vir} as the density-weighted average dark matter velocity within the virial radius. In linear theory, the peculiar velocity is defined to be the velocity of a density peak of dark matter smoothed over $10h^{-1}\text{Mpc}$. In turn, the kSZ estimate of the radial peculiar velocity is the density-weighted average gas velocity well within the virial radius, as the kSZ signal is concentrated in the central region of the cluster.

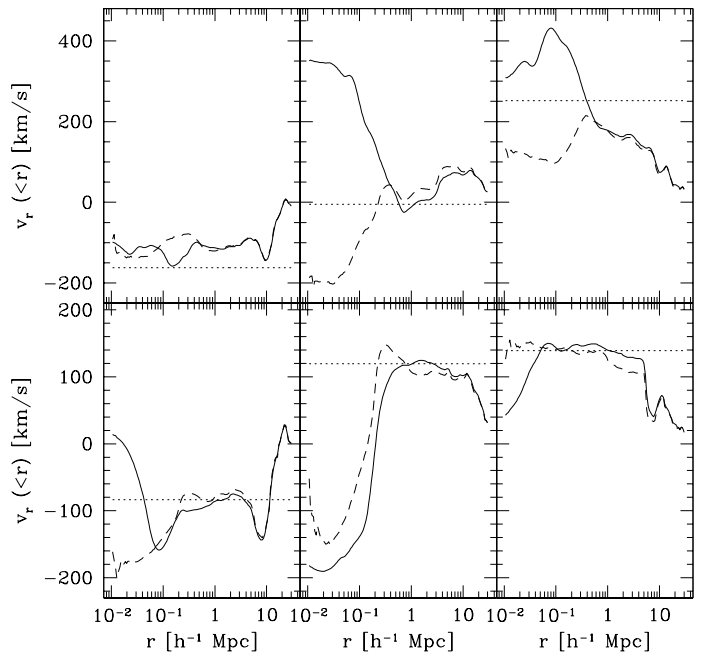


FIG. 4.— The density-weighted average radial velocities of gas (solid) and dark matter (dashed) within a sphere centered on the minimum of cluster potential for clusters at $z = 0.43$ (top) and $z = 0$ (bottom) through the same three orthogonal projections (from left to right) shown in Fig. 3. Dotted lines show the estimated radial velocity of a cluster v_r^{est} from kSZ observations; v_r^{est} is the average velocity within the aperture matched to the virial radius of the cluster. The density-weighted average velocities of gas and dark matter agree remarkably well beyond $\sim 500\text{kpc}$ (approximately half the cluster virial radius), particularly for the relaxed $z = 0$ cluster; however, the discrepancies are significant in the central region of the cluster.

To illustrate how various definitions of the peculiar velocity are related, we examine the density-weighted average gas and matter velocity profiles as a function of radius. Figure 4 shows the density-weighted average radial velocities of gas (solid) and dark matter (dashed) within a sphere centered on the minimum of the cluster potential at redshifts $z = 0.43$ (top) and $z = 0$ (bottom) through the same three orthogonal projections shown in Fig. 3. Dotted lines show the estimated radial velocity of a cluster v_r^{est} from kSZ observations; here, v_r^{est} is the average velocity within the aperture matched to the virial radius of the cluster.

The density-weighted average velocities of gas and dark matter agree remarkably well beyond $\sim 500\text{ kpc}$ (approx-

imately half of the virial radius of the cluster); however, the discrepancies are significant in the central region of the cluster. The discrepancy between the gas and dark matter velocity is most pronounced during the merger when the internal gas velocities exceed 1000 km/s. This is not surprising since dark matter and gas relax via different processes (gas through shocks and dark matter via violent relaxation). Note also that the peculiar velocity averaged within the virial radius can be significantly different from the velocity averaged over a larger scale (e.g., the difference with average velocity on $10h^{-1}$ Mpc scales reaches $\gtrsim 50\%$ in some cases). The profiles show that, contrary to common assumption, clusters do not move as solid bodies and the choice of a peculiar velocity definition is somewhat arbitrary.

4.4. The Accuracy of kSZ Peculiar Velocity Estimates

The top panel of Fig. 5 show a comparison of the estimated radial velocities of a cluster from kSZ observations v_r^{est} and the density-weighted average velocity of dark matter within the virial radius of the cluster v_r^{vir} . Here, we computed $\langle\tau^B\rangle$ directly from the simulations. We examine the simulated cluster at nine different redshifts ranging between 0.66 and 0.00, with an interval of ~ 0.8 Gyr between redshifts, and evaluate v_r^{est} and v_r^{vir} for three orthogonal projections. The time interval is roughly equal to the dynamical time of the cluster, so the various epochs provide largely independent cluster configurations. In the top panel, v_r^{est} is the aperture average velocity within an aperture matched to the virial radius r_{vir} (solid), $r_{\text{vir}}/2$ (star) and $r_{\text{vir}}/4$ (circle) of the cluster. The bottom-left panel of Fig. 5 shows a histogram of $v_r^{\text{est}} - v_r^{\text{vir}}$ for an aperture size matched to the virial radius r_{vir} (solid) and $r_{\text{vir}}/4$ (dotted-hatched).

The figure shows that the *aperture average velocity* is indeed an unbiased estimator of a radial peculiar velocity of the cluster. When the aperture encompasses the entire cluster virial region, the estimated velocity v_r^{est} agrees quite well with the true peculiar velocity of a cluster v_r^{vir} (top panel) with a small dispersion of $\lesssim 50$ km s $^{-1}$ (bottom panel). When a smaller aperture is used to select the inner region of the cluster for the analysis, the estimated velocity is still unbiased, but the errors become larger; the error is $\simeq 100$ km s $^{-1}$ if the aperture encompasses a region inside the quarter of the virial radius. The error in each measurement will depend not only on the size but also the shape of the aperture used to select the cluster region for the analysis. We consider a circular aperture for simplicity, but more elaborate apertures can be used. However, any aperture that puts more weight on the inner region of the cluster will likely lead to larger errors due to the internal bulk motions of gas at a level of ~ 200 km s $^{-1}$ present in the central region of the cluster (see Fig. 1 and Fig. 4).

The kSZ velocity estimates are in good agreement with v_r^{vir} for the cluster, with virial radii of $1.14h^{-1}$ Mpc for $z = 0.43$ and $1.26h^{-1}$ Mpc for $z = 0$; the agreement is particularly good at the lower redshift where the cluster is relaxed. This means that the various large gas velocities average to the mean cluster velocity in general, as expected from Fig. 2. However, our simulation suggests that substructure which will produce a significant velocity error occurs in a non-negligible fraction of clusters. Comparison

of high-resolution kSZ maps and X-ray maps may identify such substructure on a case-by-case basis; the extent to which the effect of subclumps can be modelled from simulations remains to be seen. Without modelling, systematic errors on the order of 50 to 100 km/s in kSZ velocity estimates will occur in some fair number of clusters, although statistically these errors should be unbiased since we are as likely to observe subclumps falling in from either side of a cluster. Maps of the kSZ effect with 1 arcminute resolution should clearly identify the clusters with potentially serious errors from subclumps.

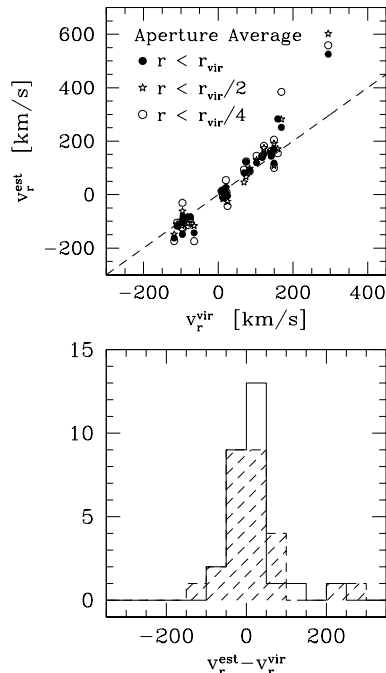


FIG. 5.— *Top*: the estimated radial velocities of a cluster from kSZ observations, v_r^{est} (Eq. (2)), are compared with the density-weighted average velocity of dark matter within the virial radius of the cluster, v_r^{vir} . We use cluster outputs at nine different redshifts ranging between 0.66 and 0.00 separated by intervals of a cluster dynamical time (~ 0.8 Gyr) and evaluate v_r^{est} and v_r^{vir} for three orthogonal projections. In the top panel, v_r^{est} is the average velocity within an aperture matched to the virial radius r_{vir} (solid), $r_{\text{vir}}/2$ (star) and $r_{\text{vir}}/4$ (circle) of the cluster. *Bottom*: a histogram of $v_r^{\text{est}} - v_r^{\text{vir}}$ for an aperture size matched to the virial radius r_{vir} (left : solid) and $r_{\text{vir}}/4$ (left : dotted-hatched). The aperture average radial velocity of a cluster from kSZ observations v_r^{est} is unbiased with a dispersion of 50 – 100 km s $^{-1}$, depending on the size of the aperture.

So far in the analysis, we used $\langle\tau^B\rangle$ derived directly from the simulations. Although this is a correct way to compute this quantity in the context of the simulation, it is not a direct observable. In practice, one needs to derive this quantity from thermal SZ effect and cluster gas temperature measurements. To mimic this situation, we performed the same analysis based on observables as described in Sec. 4.2; the results show no significant difference in scatter displayed in Fig. 5 and Fig. 6. Our conclusions therefore are not very sensitive to the details of the analysis or to the assumption of isothermality.

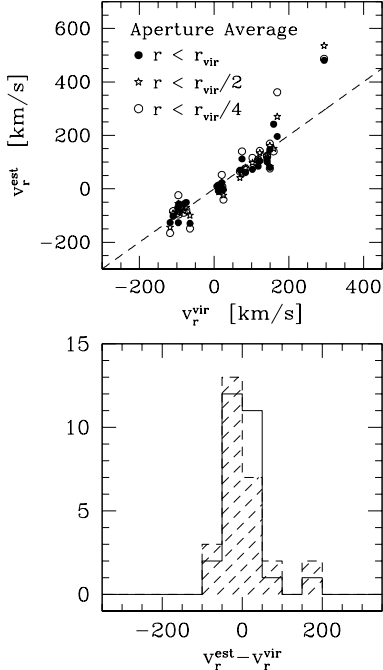


FIG. 6.— Same as Fig. 5, except that we are now computing $\langle \tau^B \rangle$ using observable quantities as described in Sec. 4.2, rather than deriving this quantity directly from the simulations. There is no significant difference between this figure and Fig. 5.

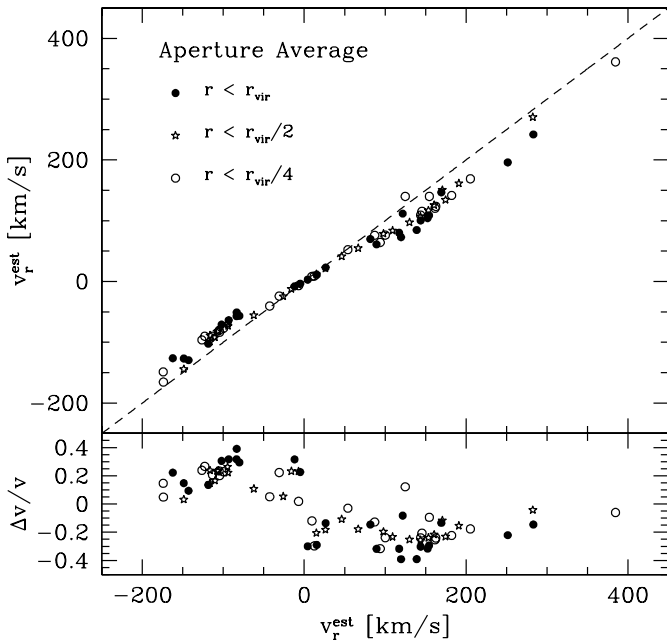


FIG. 7.— *Top*: the radial peculiar velocities estimated using observables (v_B^{est}) are compared with the values using $\langle \tau^B \rangle$ directly derived from the simulations (v_A^{est}) (see Sec. 4.2). *Bottom*: the fractional difference, $\Delta v/v = (v_B^{est} - v_A^{est})/v_A^{est}$, is plotted. The magnitude of the radial peculiar velocity measurement is systematically overestimated at a level of $\sim 20\%$ on average with a scatter of $\sim 10\%$, if we assume $\langle T_e \rangle_{n_e}^B = \langle T_X \rangle$ within each aperture. Here, the bias is caused by a monotonically increasing temperature profile toward the cluster center – this is a generic prediction of an adiabatic cluster simulation (see e.g., Frenk et al. 1999).

In the Fig. 7, we compare the estimated radial peculiar velocities derived using two different definitions of $\langle \tau^B \rangle$.

The figure shows that the magnitude of the radial peculiar velocity measurement is systematically overestimated at a level of $\sim 20\%$ on average with a scatter of $\sim 10\%$, if we assume $\langle T_e \rangle_{n_e}^B = \langle T_X \rangle$ within each aperture. Here, the bias is caused by a monotonically increasing temperature profile toward the cluster center – this is a generic prediction of adiabatic cluster simulations (see e.g., Frenk et al. 1999). The magnitude of this bias is comparable to the magnitude of scatter due to internal motions of gas in cluster cores, and the bias is systematic function of the estimated velocity rather than random (see Sec. 5 for a discussion about a more realistic estimate of this bias.)

5. DISCUSSION AND CONCLUSIONS

Using a high-resolution N-body+gasdynamic cluster simulation in a Λ CDM cosmology, we have shown that

- i Arcminute-scale kSZ measurements will provide a generally accurate (with typical errors of $\lesssim 100$ km/s) tracer of cluster peculiar velocities on scales of the cluster virial radius, but show significant discrepancies on scales smaller than half of the virial radius.
- ii In an ideal situation with an exact recovery of kSZ signal, the velocity averaged over the kSZ map pixels inside a circular aperture matched to the cluster virial region provides a statistically unbiased estimate of a cluster’s radial peculiar velocity with a small dispersion of $\lesssim 50$ km s $^{-1}$. When analyzing an actual kSZ map with noise, one may want to use a smaller aperture to include only the region of the map with higher signal-to-noise; in such case, the velocity measurement is still unbiased, but with larger errors.
- iii While accurate cluster velocity estimates might be obtained in a statistical sense from kSZ estimates, any individual cluster can give a significant velocity error due to random subclumps with velocities along the line of sight. Comparisons of high-resolution kSZ and X-ray maps can identify such subclumps, although it is unclear how accurately their effect can be modelled on a case-by-case basis.

Our estimated error amplitude agrees with the conclusions of Holder (2002). Although our analysis shows that the accurate measurements of radial peculiar velocity of clusters are possible, careful observational and theoretical studies of potential biases are required before we can use the kSZ peculiar velocity measurements to extract cosmological information.

Observationally, one needs thermal SZ effect and cluster gas temperature measurements to determine the beam-smearred column density, $\langle \tau^B \rangle = (m_e c^2 / \sigma_T k_B) \times [\langle y^B \rangle / \langle T_e \rangle_{n_e}^B]$. However, the density-weighted electron temperature $\langle T_e \rangle_{n_e}^B$ is not an observable; instead, the emission-weighted temperature of cluster gas $\langle T_X \rangle$ from the X-ray spectroscopy is often used. If the intracluster medium is isothermal throughout, then $\langle T_e \rangle_{n_e}^B = \langle T_X \rangle$. However, this is clearly an incorrect assumption: recent high-resolution X-ray cluster observations revealed the non-isothermality of the intracluster medium (Markevitch et al. 1998; Peterson et al. 2001; Tamura et al. 2001; De Grandi & Molendi 2002). Nevertheless, in the absence of

a theoretical model of temperature structure, the isothermality assumption is likely an unavoidable one in the analysis of the real observations, particularly for distant clusters where detail temperature structure is difficult to study. Clearly, such an incorrect assumption could introduce an additional bias in the kSZ measurements of the cluster peculiar velocity. Using the high-resolution adiabatic simulation used in this paper, we find that the use of $\langle T_X \rangle$ leads to overestimate of the inferred peculiar velocity measurement at the maximum level of $\sim 20\%$ due to monotonically increasing temperature profile toward the cluster center. Yoshikawa et al. (1998), on the other hand, reported that the use of $\langle T_X \rangle$ leads to underestimate of similar magnitude due to temperature drop in the center of the simulated cluster in their rather low-resolution adiabatic cluster simulations. However, the real clusters (e.g., De Grandi & Molendi 2002) and clusters simulated with starformation and cooling (e.g., Valdarnini 2002) seem to have more isothermal core than the simulated cluster analyzed here and this bias will be correspondingly smaller. Further analyses using simulations with cooling and starformation are needed to evaluate the effect, while reproducing the observed temperature profiles of clusters.

The Sunyaev-Zeldovich effect is independent of redshift and unable to distinguish between objects at different redshifts along the same line of sight. While the chance of two massive galaxy clusters being aligned is negligible (Voit et al. 2001), the probability for random alignment of a galaxy group ($M \simeq 10^{13}$ to $10^{14} M_\odot$) with a cluster will be somewhat higher and will appear like additional substructure in the kSZ map. If the group has a large line-of-sight velocity with the same sign as the cluster peculiar velocity, it will be detectable in the same way as a high-velocity merging subclump, and might be modelled out in the same way. Groups with smaller peculiar velocities will bias the velocity determination and be harder to pick out in the kSZ maps. This systematic error will be small, considering that the high-velocity merging subclump in our simulation biases the velocity determination by around 50 km/s and a random galaxy will give a substantially smaller signal. This estimate is consistent with an assessment of this effect by Aghanim et al. (2001) who argue that random superposition of clusters with other objects along the line of sight leads to typical *rms* velocity errors of $\lesssim 100$ km/s. A more accurate estimation of this bias requires modelling with large-volume simulations.

We mention in passing that significant internal bulk velocities with characteristic amplitudes of 100 to 300 km/sec will greatly complicate measurements of cluster rotations with characteristic kSZ signals at the μK level, as proposed by Cooray & Chen (2002). A realistic assessment of this effect would need to use high-resolution simulated clusters, such as the one studied here.

Measuring blackbody kSZ distortions at the few μK level of course requires overcoming other systematics unrelated to the kSZ signal itself. Most importantly, galaxy clusters will possess a dominant thermal Sunyaev-Zeldovich distortion much larger than the kSZ signal. This thermal signal can, to some extent, be extracted via its departure

from a blackbody spectrum using multiple frequency measurements, but relativistic corrections (Rephaeli 1995; Itoh et al. 2001) or departures from kinetic equilibrium (Blasi et al. 2000) can complicate this analysis (see Holder 2002). Second, the blackbody kSZ distortion must be separated from the blackbody primary temperature fluctuations of the microwave background. This can be accomplished via spatial filtering, since the primary microwave background fluctuations possess little power on cluster scales. The errors in filtering will give some unavoidable systematic error. Detailed simulations of the filtering process were done by Haehnelt & Tegmark (1996) and updated for currently envisioned experimental capabilities by Holder (2002).

Aghanim et al. (2001) apply a simple filter to simulated Planck satellite maps, finding velocity errors due to the filtering of 300 to 600 km/s due to Planck's angular resolution. Upcoming ground-based experiments are likely to have higher sensitivity and resolution than Planck, although with complications from atmospheric emission. The extent to which the kSZ signal can be isolated from the background fluctuations in arcminute resolution maps at high sensitivity needs to be studied in more detail. We anticipate systematic errors comparable to those from internal motions. Galactic dust emission and radio point sources are unlikely to be major problems at 200 GHz frequencies and arcminute angular scales, but lensed images of distant dusty galaxies could contribute a significant confusion noise (Blain 1998) and may need to be imaged at higher frequencies to extract the kSZ signal accurately.

Our simulated galaxy cluster shows that, perhaps contrary to naive expectation, the internal bulk flows in galaxy clusters do not present an insurmountable source of systematic error for peculiar velocity estimates based on the kinematic Sunyaev-Zeldovich effect. Aperture-averaged velocity estimates are largely unbiased. High-velocity subclumps merging with the cluster along the line of sight will induce systematic errors, but many of these clumps can be identified as particularly bright kSZ signals, and can be removed via comparison with X-ray maps. It is not unreasonable to hope that SZ cluster surveys will eventually produce cluster peculiar velocity catalogs with systematic velocity errors at a level of 50 km/s independent of the cluster distance. Velocity catalogs of such accuracy would provide a powerful probe of the growth of structure in the mildly nonlinear regime.

We would like to thank Lloyd Knox for useful discussion and comments, and Roman Juszkiewicz for asking questions prompting this study. The work presented here was partially supported by NASA through a Hubble Fellowship grant from the Space Telescope Science Institute, which is operated by the Association of Universities for Research in Astronomy, Inc., under NASA contract NAS5-26555 and by NSF through funding of the Center for Cosmological Physics at the University of Chicago (NSF PHY-0114422). DN thanks John Carlstrom for his support through NASA LTSA grant NAG5-7986. AK is a Cottrell Scholar of the Research Corporation and is supported by NASA's SARA program through grant NAG5-10110.

REFERENCES

- Aghanim, N., Górski, K. M., & Puget, J.-L. 2001, *A&A*, 374, 1
- Bahcall, N. A., Gramann, M., & Cen, R. 1994, *ApJ*, 436, 23
- Birkinshaw, M. 1999, *Phys. Rep.*, 310, 97
- Blain, A. W. 1998, *MNRAS*, 297, 502
- Blasi, P., Olinto, A. V., & Stebbins, A. 2000, *ApJ*, 535, L71
- Branchini, E., Freudling, W., Da Costa, L. N., Frenk, C. S., Giovanelli, R., Haynes, M. P., Salzer, J. J., Wegner, G., & Zehavi, I. 2001, *MNRAS*, 326, 1191
- Carlstrom, J. E., Holder, G. P., & Reese, E. D. 2002, *ARA&A*, 40, 643
- Colin, P., Klypin, A. A., & Kravtsov, A. V. 2000, *ApJ*, 539, 561
- Colberg, J. M., White, S. D. M., Yoshida, N., MacFarland, T. J., Jenkins, A., Frenk, C. S., Pearce, F. R., Evrard, A. E., Couchman, H. M. P., Efstathiou, G., Peacock, J. A., Thomas, P. A., & The Virgo Consortium. 2000, *MNRAS*, 319, 209
- Cooray, A. & Chen, X. 2002, *ApJ*, 573, 43
- Croft, R. A. C. & Efstathiou, G. 1994, *MNRAS*, 268, L23
- da Costa, L. N., Nusser, A., Freudling, W., Giovanelli, R., Haynes, M. P., Salzer, J. J., & Wegner, G. 1998, *MNRAS*, 299, 425
- De Grandi, S. & Molendi, S. 2002, *ApJ*, 567, 163
- Diego, J., Hansen, S., & Silk, J. 2002, *MNRAS*, submitted (*astro-ph/0207178*)
- Doré, O., Knox, L., & Peel, A. 2002, *ApJ*, submitted (*astro-ph/0207369*)
- Frenk, C. S., White, S. D. M., Bode, P., Bond, J. R., Bryan, G. L., Cen, R., Couchman, H. M. P., Evrard, A. E., Gnedin, N., Jenkins, A., Khokhlov, A. M., Klypin, A., Navarro, J. F., Norman, M. L., Ostriker, J. P., Owen, J. M., Pearce, F. R., Pen, U. ., Steinmetz, M., Thomas, P. A., Villumsen, J. V., Wadsley, J. W., Warren, M. S., Xu, G., & Yepes, G. 1999, *ApJ*, 525, 554
- Freudling, W., Zehavi, I., da Costa, L. N., Dekel, A., Eldar, A., Giovanelli, R., Haynes, M. P., Salzer, J. J., Wegner, G., & Zaroubi, S. 1999, *ApJ*, 523, 1
- Haehnelt, M. G. & Tegmark, M. 1996, *MNRAS*, 279, 545
- Holder, G. P. 2002, *ApJ*, To be submitted (*astro-ph/0207600*)
- Holzappel, W. L., Arnaud, M., Ade, P. A. R., Church, S. E., Fischer, M. L., Mauskopf, P. D., Rephaeli, Y., Wilbanks, T. M., & Lange, A. E. 1997, *ApJ*, 480, 449
- Itoh, N., Kawana, Y., Nozawa, S., & Kohyama, Y. 2001, *MNRAS*, 327, 567
- Jing, Y. P. & Boerner, G. 1998, *ApJ*, 503, 502
- Juszkiewicz, R., Springel, V., & Durrer, R. 1999, *ApJ*, 518, L25
- Kashlinsky, A. & Atrio-Barandela, F. 2000, *ApJ*, 536, L67
- Klypin, A., Kravtsov, A. V., Bullock, J. S., & Primack, J. R. 2001, *ApJ*, 554, 903
- Kravtsov, A. V. 1999, Ph.D. Thesis
- Kravtsov, A. V., Klypin, A., & Hoffman, Y. 2002, *ApJ*, 571, 563
- Lange, A. E., Church, S. E., & Holzappel, W. 1998, *American Astronomical Society Meeting*, 30, 908
- Markevitch, M., Forman, W. R., Sarazin, C. L., & Vikhlinin, A. 1998, *ApJ*, 503, 77
- Markevitch, M., Ponman, T. J., Nulsen, P. E. J., Bautz, M. W., Burke, D. J., David, L. P., Davis, D., Donnelly, R. H., Forman, W. R., Jones, C., Kaastra, J., Kellogg, E., Kim, D. ., Kolodziejczak, J., Mazzotta, P., Pagliaro, A., Patel, S., Van Speybroeck, L., Vikhlinin, A., Vrtilik, J., Wise, M., & Zhao, P. 2000, *ApJ*, 541, 542
- Markevitch, M., Vikhlinin, A., & Forman, W. R. 2002, To appear in *ASP Conference Series*, (*astro-ph/0208208*)
- Mazzotta, P., Fusco-Femiano, R., & Vikhlinin, A. 2002, *ApJ*, 569, L31
- Nagai, D. & Kravtsov, A. V. 2002, *ApJ*, submitted (*astro-ph/0206469*)
- Norman, M. L. & Bryan, G. L. 1999, in *The radio galaxy Messier 87 : proceedings of a workshop held at Ringberg Castle, Tegernsee, Germany, 15-19 September 1997 / Hermann-Josef Röser, Klaus Meisenheimer, eds. Berlin ; New York : Springer, 1999. (Lecture notes in physics, 530, ISSN0075-8450).*, p.106, 106
- Peel, A. & Knox, L. 2002, To appear in *Proceedings of Dark Matter 2002*, (*astro-ph/0205438*)
- Peterson, J. R., Paerels, F. B. S., Kaastra, J. S., Arnaud, M., Reiprich, T. H., Fabian, A. C., Mushotzky, R. F., Jernigan, J. G., & Sakelliou, I. 2001, *A&A*, 365, L104
- Rephaeli, Y. 1995, *ApJ*, 445, 33
- Raymond, J. C. & Smith, B. W. 1977, *ApJS*, 35, 419
- Ricker, P. M. & Sarazin, C. L. 2001, *ApJ*, 561, 621
- Sun, M. & Murray, S. S. 2002, To appear in *ApJ*, Vol 576, 2002, (*astro-ph/0206255*)
- Sunyaev, R. A. & Zel'dovich, Y. B. 1980, *ARA&A*, 18, 537
- Tamura, T., Kaastra, J. S., Peterson, J. R., Paerels, F. B. S., Mittaz, J. P. D., Trudolyubov, S. P., Stewart, G., Fabian, A. C., Mushotzky, R. F., Lumb, D. H., & Ikebe, Y. 2001, *A&A*, 365, L87
- Valdarnini, R. 2002, *ApJ*, 567, 741
- Vikhlinin, A., Markevitch, M., & Murray, S. S. 2001, *ApJ*, 551, 160
- Voit, G. M., Evrard, A. E., & Bryan, G. L. 2001, *ApJ*, 548, L123
- Yoshikawa, K., Itoh, M., & Suto, Y. 1998, *PASJ*, 50, 203
- Zeldovich, Y. B. & Syunayev, R. A. 1969, *Ap&SS*, 4, 301